JOURNAL OF CATALYSIS 48, 177–193 (1977)

An Analysis of the Fouling of Catalyst Pellets under Nonisothermal Conditions

P. A. RAMACHANDRAN, E. K. T. KAM, AND R. HUGHES

Department of Chemical Engineering, University of Salford, Salford, M5 4WT, England

Received March 24, 1976; revised October 26, 1976

An analysis of the influence of heat and mass diffusion on the fouling of a single catalyst pellet has been made for generalized Langmuir–Hinshelwood kinetics and for parallel and series fouling. The influence of the various parameters affecting catalyst activity including the Thiele modulus of the main reaction, the heats of adsorption and the activation energies of the main and deactivating reactions have been examined. The nature of fouling under conditions where multiple steady states can occur within the catalyst is also considered.

INTRODUCTION

The analysis of the problem of catalyst fouling is important in the design and operation of many heterogeneous reactors. Some examples of industrial processes where the catalyst becomes fouled are the cyclization of aliphatic hydrocarbons (*1*), the cracking of gas oil (*2*) and cumene (*3*), polymerization of olefins (*4*) and hydrogenation (*5*) and dehydration (*6*) reactions. The situation where the catalyst loses activity due to volatilization of active component [for example $HgCl_2$ deposited on activated carbon (*7*)] can also be analyzed similarly. The thermal denaturation of immobilized enzymes can be modeled on lines parallel to nonisothermal fouling of catalyst pellets (*8*) and the present work will also have applications in this area. A number of theoretical investigations have dealt with isothermal fouling of catalysts (*9–15*) but the main reaction is often accompanied by large heat effects and this often causes significant intraparticle temperature gradients which affect the rate of both main and fouling reactions. Sagara *et al.* (*16*) have analyzed fouling for nonisothermal systems where both the main reaction and the fouling reaction are of first order. However, the kinetics of the main reaction may often be best described by a Langmuir–Hinshelwood kinetic expression. In the present paper, the general problem of fouling of catalysts under nonisothermal reaction conditions but excluding external heat and mass transfer resistances is analyzed and the influence of various factors affecting the catalyst fouling is critically examined. Parallel, series and parallel/series fouling processes are analyzed where first order kinetics with respect to the fouling precursor and the concentration of activity sites are assumed.

NOMENCLATURE

a	dimensionless concentration of A
b	dimensionless concentration of B
C_A, C_B	concentrations of A and B
De_A, De_B	effective diffusivities of A and B
E, E_f	activation energies of the main, and fouling reaction
ΔH	heat of reaction of the main reaction

ISSN 0021-9517

$\left.\begin{matrix}\Delta H_A,\\ \Delta H_B\end{matrix}\right\}$ heats of adsorption of A and B

h_{K_A}, h_{K_B} dimensionless heats of adsorption of A and B, $-\Delta H_A/R_gT_0$ and $-\Delta H_B/R_gT_0$

k reaction constant of the main reaction

K_A, K_B adsorption equilibrium constants for A and B

K_A^*, K_B^* dimensionless adsorption equilibrium constants for A and B, $K_AC_{A_0}$, $K_BC_{A_0}$

k_e thermal conductivity of the catalyst

k_f rate constant for fouling reaction

r radial coordinate in the pellet

R radius of the catalyst pellet

R_g gas constant

t reaction time

T temperature

S activity

β dimensionless heat of reaction parameter or thermicity $(-\Delta H)\mathrm{De_A}C_{A_0}/k_eT_0$

γ, γ_f dimensionless activation energies for the main and fouling reaction E/R_gT_0 and E_f/R_gT_0

δ dimensionless radial coordinate in the pellet, r/R

η effectiveness factor at any time

η_0 effectiveness factor at time ($\tau = 0$)

θ dimensionless temperature

$\bar{\theta}$ mean dimensionless temperature

ϕ Thiele modulus for the main reaction, $R(k/\mathrm{De_A})^{\frac{1}{2}}$

τ dimensionless time, $tk_{f_1}C_{A_0}$

Subscripts

0 bulk gas phase condition

1 parallel fouling

2 series fouling

GENERAL THEORY

The general theory has been described in a previous paper on isothermal fouling (*14*). For nonisothermal cases, an additional equation for the energy balance has to be incorporated into the model. The reaction system is assumed to be of the following type:

$A \rightarrow B + C$ main reaction,

$A \rightarrow$ coke parallel deactivation,

$B \rightarrow$ coke series deactivation.

The concentration and temperature distribution of A within the pellet can be expressed by the following dimensionless equations,

$$\nabla^2 a - \phi^2 f(a, \theta, S) = 0, \tag{1}$$

$$\nabla^2 \theta + \beta\phi^2 f(a, \theta, S) = 0, \tag{2}$$

and the rate of deactivation can be assumed to be given by the following general relation,

$$-\frac{dS}{d\tau} = g_1(a, \theta, S) + \frac{k_{f_2}}{k_{f_1}} g_2(b, \theta, S), \tag{3}$$

which can be used for either parallel or series fouling or a combination of both by substituting appropriate values for the rate constants for parallel (k_{f_1}) and series (k_{f_2}) fouling. An assumption implicitly made in Eq. (1) is that the fouling reaction rate is very small in comparison with the main reaction and hence the amount of A consumed in the deactivation reaction does not appear in the mass balance equation for A. The concentration of the reactant A and the product B can be related stoichiometrically by

$$b = b_0 + \frac{\mathrm{De_A}}{\mathrm{De_B}}(1 - a). \tag{4}$$

Further, the concentration A and the intraparticle temperature can be related by Prater's equation (*17*) as

$$\theta = 1 + (1 - a)\beta. \tag{5}$$

With this simplification, Eq. (1) becomes

$$\nabla^2 a - \phi^2 f_1(a, S) = 0. \tag{6}$$

The boundary conditions at any τ assuming no external resistances are:

$$\text{at} \quad \delta = 0, \quad \frac{da}{d\delta} = \frac{d\theta}{d\delta} = 0, \qquad (7)$$

$$\delta = 1, \quad a = \theta = 1.$$

And the initial condition at any δ is

$$\tau = 0; \quad S = 1. \qquad (8)$$

The problem now reduces to solving Eqs. (3) and (6) to evaluate the concentration profile of A and the catalytic activity in the pellet. The results can be represented in terms of the effectiveness factor which is now defined as the ratio of the rate of reaction at any given time to the rate for an unfouled catalyst with no diffusional resistance.

The specific kinetics assumed in this paper take the following form for the main reaction

$$f(a, \theta, S) = \frac{aS \exp[(\gamma - h_{K_A})(1 - 1/\theta)]}{1 + K_A{}^* a \exp[-h_{K_A}(1 - 1/\theta)] + K_B{}^* b \exp[-h_{K_B}(1 - 1/\theta)]}, \qquad (9)$$

and for the fouling reaction

$$-\frac{dS}{d\tau} = aS \exp[\gamma_{f_1}(1 - 1/\theta)] + (k_{f_2}/k_{f_1})bS \exp[\gamma_{f_2}(1 - 1/\theta)]. \qquad (10)$$

The equations were solved using the orthogonal collocation method of Villadsen and Stewart (*18*) using six interior collocation points. Details of the procedure when applied to catalyst fouling have been given in a previous publication (*14*).

RESULTS AND DISCUSSION

In order to check the accuracy of the orthogonal collocation method, the results obtained by this method were compared with the numerical solutions of Sagara *et al.* (*16*) for first order kinetics in both the main and fouling reactions. The latter based their numerical solution on a quasi-linearization technique. It was found that the plots of effectiveness factor against fouling time were identical for both methods.

When nonisothermal fouling is considered, the number of parameters capable of influencing the behavior of the system is markedly increased compared with isothermal conditions. Thus, in addition to the heat of reaction parameter, β, and activation energy parameter, γ, for the main reaction the activation energy for the fouling reaction must be taken into account by including the appropriate term, γ_f. Also, when Langmuir–Hinshelwood type kinetics are observed, then the adsorption constants $K_A{}^*$ and $K_B{}^*$ and their variation with temperature (using the appropriate heats of adsorption h_{K_A} and h_{K_B}) should also be included in the analysis. A system incorporating all possible variations of these parameters would be extremely complex and would be very time-consuming to investigate in comprehensive detail. The results presented here show the main conclusions for the variation of these parameters and the aim has been to determine which are the most important additional factors which need to be considered when nonisothermal fouling occurs. As before (*14*), the three modes of fouling have been taken as parallel, series or a combination of parallel and series fouling.

Comparison between Isothermal and Nonisothermal Fouling

The contrast between isothermal and nonisothermal operation of a catalyst undergoing fouling by a parallel reaction

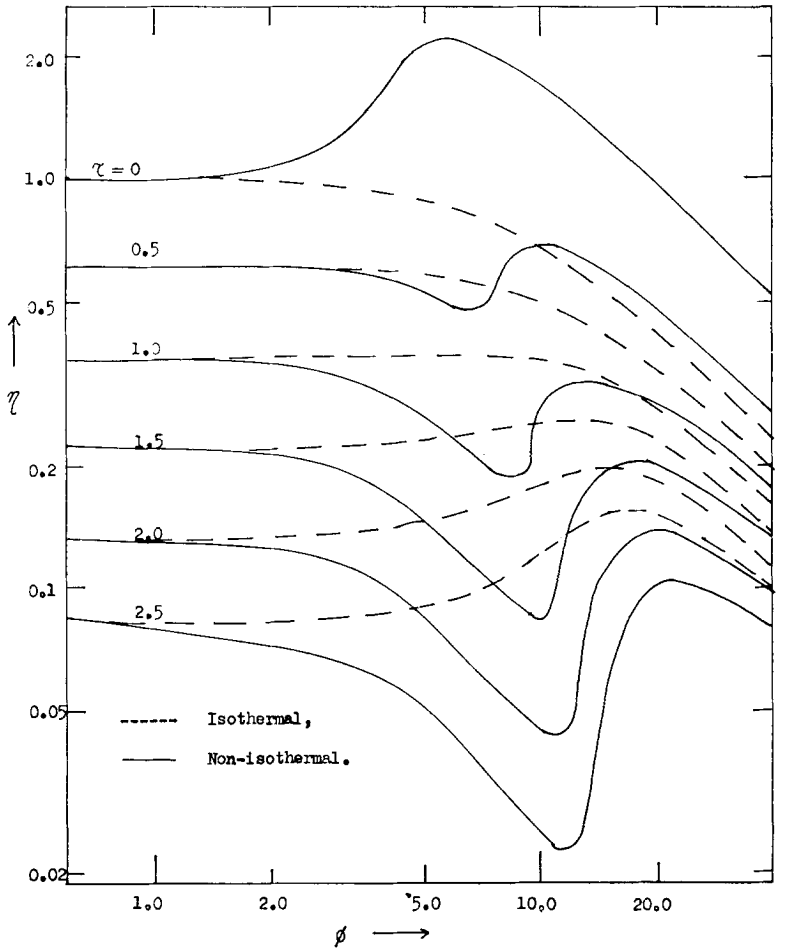

FIG. 1. Parallel fouling. Comparison of nonisothermal and isothermal particle effectiveness factors. Data $\gamma = \gamma_f = 20$, $\beta = 0.2$, $K_A^* = K_B^* = 10$, $b_0 = 0$, $h_{K_A} = h_{K_B} = 5$. (for isothermal fouling, $\gamma = \gamma_f = \beta = 0$.)

mechanism is shown in Fig. 1. In this plot of effectiveness factor against Thiele modulus with the dimensionless fouling time τ as parameter, a value of 0.2 was taken for the thermicity factor β and equal values of the activation energy for the main and fouling reaction were assumed. For small values of the Thiele modulus ($\phi < 2$) the curves for isothermal and nonisothermal operation are almost identical and fouling tends to be uniform throughout the pellet due to the absence of significant diffusional and thermal resistances within the pellet. For values of ϕ greater than 2 a nonuniform fouling pattern develops within the catalyst pellet and for large values of ϕ the fouling is confined to a region close to the catalyst surface. As shown in Fig. 1, for fouling times τ up to about 2.5 the nonisothermal pellet gives a minimum followed by a maximum in the η vs ϕ plots before the asymptotic region is attained. For the same range of fouling time the isothermal pellet shows a monotonic decrease of η with increasing ϕ. At larger times on stream, however, a slight maximum develops in the isothermal curves at values of the Thiele modulus close to 10, which may in some cases exceed the equivalent nonisothermal maximum at this point. In no case of

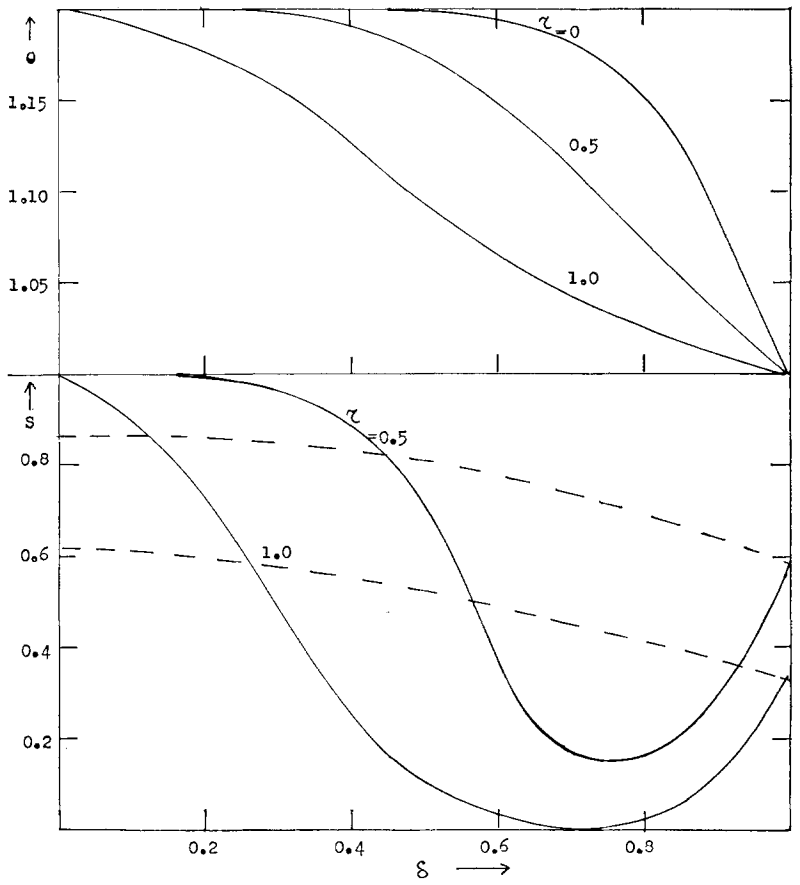

FIG. 2. Parallel fouling. Temperature profiles and distribution of active sites within a pellet. Data: $\gamma = \gamma_f = 20$, $\beta = 0.2$, $K_A^* = K_B^* = 10$, $b_0 = 0$, $h_{K_A} = h_{K_B} = 5$, and $\phi = 10$. (for isothermal fouling, $\gamma = \gamma_f = \beta = 0$.)

isothermal operation was a minimum observed in the effectiveness factor curve. Because of these features care must be exercised in the selection of an operating region for the catalyst.

Corresponding temperature and activity profiles (in terms of the concentration of active sites, S) for a value of ϕ equal to 10 are given in Fig. 2. These demonstrate the steep minimum in the activity close to the catalyst surface compared to the more uniform decrease of activity towards the catalyst surface observed under isothermal conditions. For isothermal conditions the minimum activity is at the surface; for nonisothermal conditions this (lower) minimum is close to the surface but extends further into the pellet with increased fouling time. Note that the surface activity concentrations for both cases are very close because the value of temperature and concentration are unity at the surface, consistent with the boundary conditions adopted.

A similar comparison between isothermal and nonisothermal conditions may be made for series fouling for the same parameters as were studied for parallel fouling. Figure 3 shows that at low ϕ values the effectiveness factors are greater for the nonisothermal case compared with the isothermal one. Nevertheless, when ϕ is

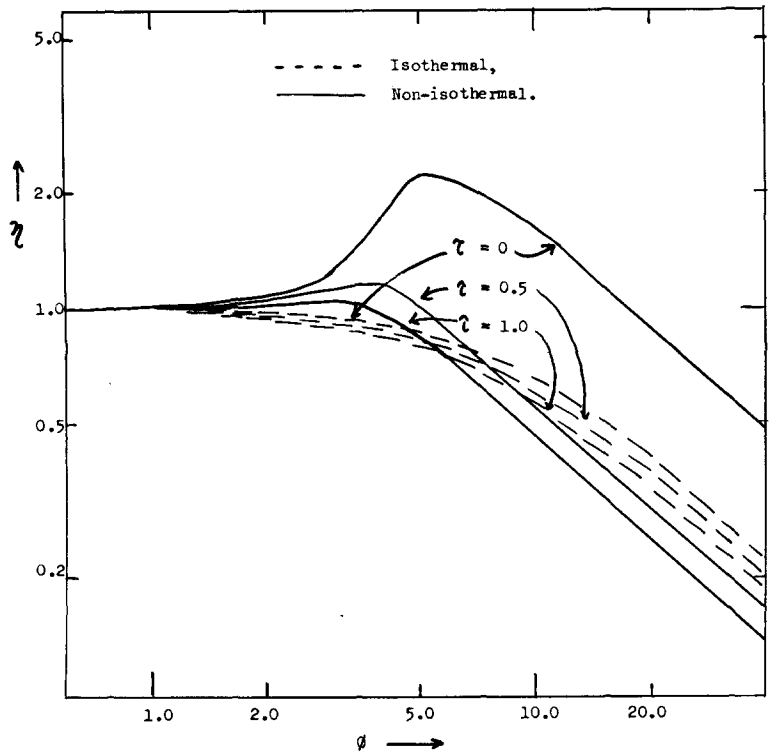

FIG. 3. Effect of thermicity, series fouling. Comparison of nonisothermal and isothermal effectiveness factors. Data: $\gamma = 20$, $\gamma_f = 20$, $\beta = 0.2$, $K_A^* = 10$, $K_B^* = 10$, $b_0 = 0$, $h_{K_A} = 5$, $h_{K_B} = 5$. (for isothermal fouling, $\gamma = \gamma_f = \beta = 0$.)

greater than about 10 this situation is reversed even for relatively small fouling periods. The corresponding activity plot is given in Fig. 4. No minimum in the activity with radial position is observed now and the nonisothermal activity profiles after fouling periods of 0.5 are very steep near the pellet surface. In addition, after fairly rapid initial fouling the effect of increased fouling time becomes only slightly more significant for longer periods for nonisothermal series fouling compared to isothermal series fouling.

The reason for the apparent better performance of fouled catalysts operating under isothermal conditions at moderate values of the Thiele modulus may be explained in terms of the effectiveness factor plots in Figs. 1 and 3. For small fouling times the effectiveness factor plots give a maximum for both parallel and for series fouling at Thiele moduli between about 5 and 10. This high value of the effectiveness factor for the main reaction is caused by the temperature rise in the pellet and since the activation energies of both main and fouling reactions are assumed equal in these figures, the acceleration of the main reaction by this increase in temperature is accompanied by a corresponding increase in fouling. As time progresses, this fouling deposit causes a rapid decrease in activity compared with the isothermal case and ultimately the nonisothermal effectiveness becomes less than if isothermality had been preserved throughout the deactivation period. If γ_f were lower than γ, this effect would be lessened. These comments apply, of course, only for the absence of film resistances. Incorporation of these may

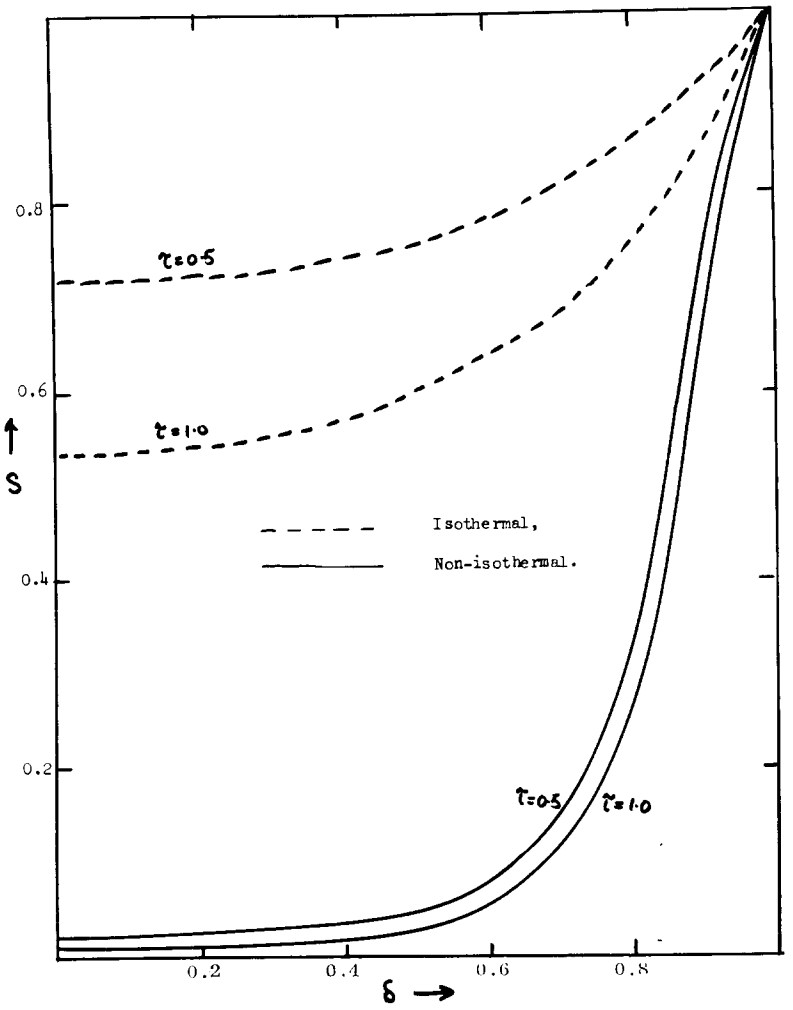

FIG. 4. Series fouling; active sites distribution. Data: $\gamma = \gamma_f = 20$, $\beta = 0.2$, $K_A^* = K_C^* = 10$, $h_{K_A} = h_{K_C} = 5$, $b_0 = 0$, and $\phi = 5$. (for isothermal fouling, $\gamma = \gamma_f = \beta = 0$.)

modify the effectiveness factors of the pellet.

All the above results are concerned with exothermic reactions. Endothermic processes under the same conditions but with the sign of the thermicity factor reversed ($\beta = -0.2$) are shown in Fig. 5 for pellet effectiveness and Fig. 6 for pellet activity and temperature profiles. Figure 5 shows that for parallel fouling the effectiveness factor curves have, as might be expected, a shape very similar to those for isothermal operation. For series fouling, however, deactivation is now much diminished with fouling time. A comparison of the curves for isothermal and endothermic effectiveness factors shows that although slightly lower absolute values are obtained for the pellet effectiveness the corresponding relative deactivation by fouling is less than that for isothermal conditions. Figure 6 shows that with endothermic fouling the temperatures inside the pellet increase slightly with fouling time and this is accompanied by an increase in reactant concentration within the pellet. For parallel fouling this will lead to increased deactivation since fouling depends on reactant

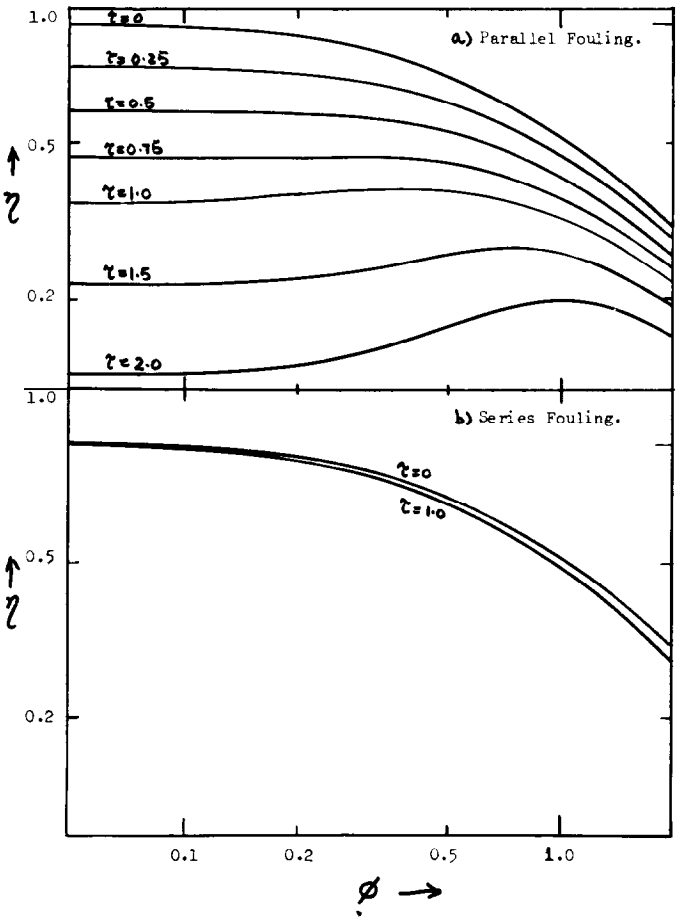

FIG. 5. η vs ϕ plots, endothermic reactions. Effectiveness factor plots for parallel and series fouling. Data: $\gamma = \gamma_f = 20$, $\beta = -0.2$, $K_A^* = K_B^* = 10$, $h_{K_A} = h_{K_B} = 10$, $b_0 = 0$.

concentration, but for series fouling the product concentration will be diminished thus causing a decrease in the rate of deactivation of the catalyst.

For packed bed reactors or for differential reactors operated with recycle there will be significant quantities of product in the bulk gas. The effect of a finite concentration of product gas in the inlet gas stream was considered by taking the recycle constant b_0 in Eq. (4) equal to 0.25. The results obtained are shown in Fig. 7 for series and parallel/series fouling, other conditions being the same as were used in previous figures. Parallel fouling is unaffected by product present in the bulk gas, whereas in both series and series/parallel fouling the deactivation becomes significant even for very low values of the Thiele modulus.

Khang and Levenspiel (*15*) have suggested that for first order isothermal systems a simple power law expression can be used to describe the deactivation phenomena. The index of deactivation was found to depend on the Thiele modulus for the main reaction, varying from unity for a uniformly deactivated pellet to a value as high as 3 for a shell deactivation process. An attempt was made to use this form of analysis for the nonisothermal system described in this paper but the values of the index of deactivation oscillated between 1 to 2 even for a first order parallel

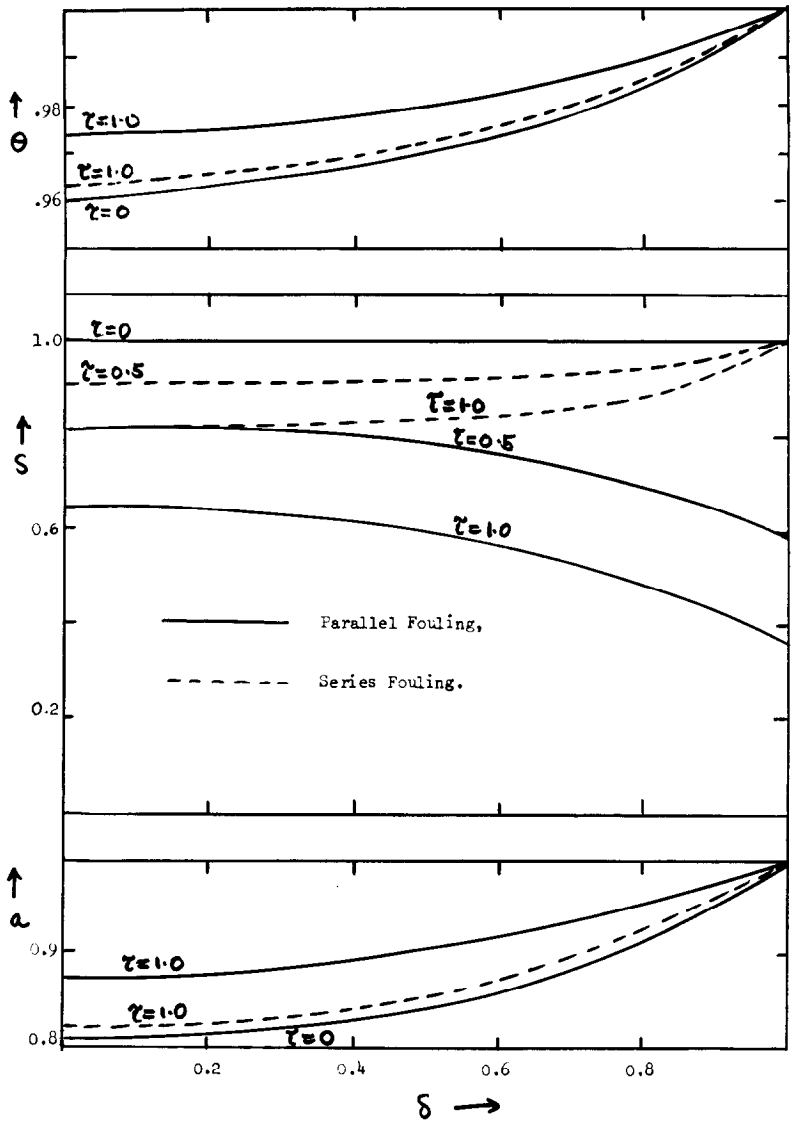

FIG. 6. Endothermic reactions. Intrapellet distribution of temperature, activity and concentration. Data: $\gamma = \gamma_f = 20$, $\beta = -0.2$, $K_A^* = K_B^* = 10$, $b_0 = 0$, $h_{K_A} = h_{K_B} = 5$, $\phi = 5$.

fouling process and for series fouling the index varied from infinity to 0.5. Thus a simple power law correlation does not seem adequate to describe nonisothermal deactivation.

Effect of Thermal Parameters on Catalyst Fouling

The effect of temperature rise during reaction, as represented by the thermicity factor β, and variations in the ratio of γ to γ_f, on the catalyst effectiveness is illustrated in Fig. 8a and b for parallel and series fouling, respectively. In these figures the effectiveness factor is plotted against β for a constant value of the Thiele modulus ($\phi = 10$) with the ratio γ_f/γ as parameter. Figure 8 shows that with parallel fouling the effectiveness factor curves can be divided into two regions. For $\gamma_f/\gamma = 0.5$ the effectiveness factor

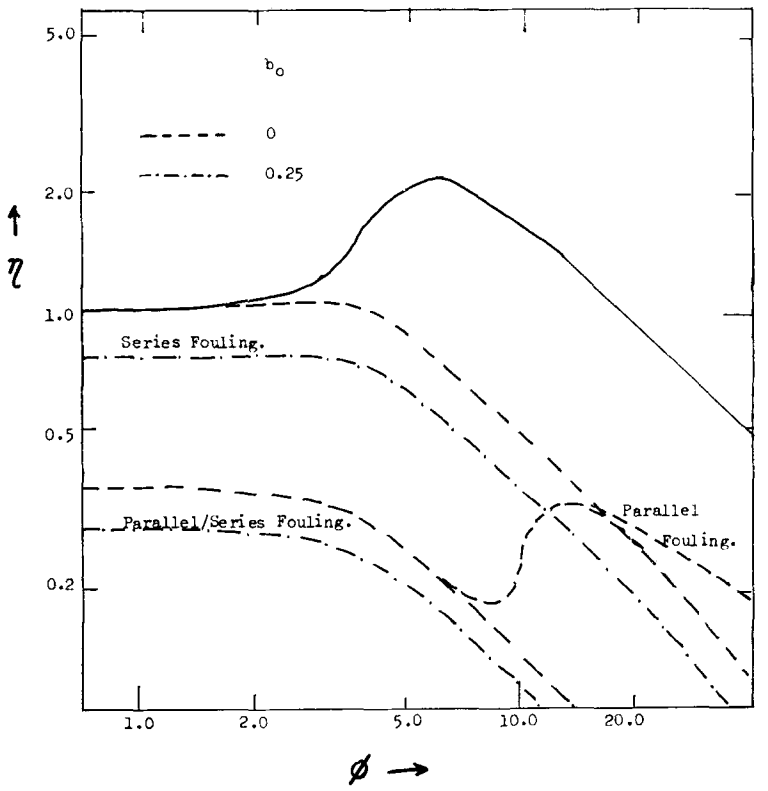

FIG. 7. Effect of b_0. Effect of a finite product concentraton on nonisothermal fouling. Data: $\gamma = \gamma_f = 20$, $\beta = 0.2$, $K_A^* = K_C^* = 10$, $h_{K_A} = h_{K_C} = 5$.

follows a similar pattern to that obtained with no deactivation, i.e., the effectiveness factor increases with increasing values of β. However, when the ratio γ_f/γ is unity or greater, the effectiveness factor goes through a slight maximum and then decreases sharply with increasing β. The results for series fouling in Fig. 8b show that significant catalyst deactivation can now occur even for γ_f/γ equal to 0.5 and that most of the catalyst fouling occurs in the early stages of reaction. There is only a marginally greater deactivation at higher values of γ_f/γ and at increased fouling times. This rapid initial rate of fouling seems to be typical of series deactivation under nonisothermal conditions. For low values of the Thiele modulus the effects of both β and γ_f/γ are insignificant.

The influence of the variation of activation energy of the main reaction is shown in Fig. 9a and b. Three values of the Thiele modulus are considered, namely $\phi = 1$, 5, and 10. In all cases γ_f and β are held constant at 20 and 0.2, respectively. The effectiveness factor is now plotted as the ratio η/η_0 (where η_0 is the pellet effectiveness factor at $\tau = 0$) against the fouling time τ and therefore the curves denote the relative decrease in catalyst effectiveness with time. Curves for values of γ equal to 10, 20, and 30 at values of ϕ equal to 1, 5, and 10 are shown in these figures. At small values of ϕ ($\phi \leqslant 1$) the results show that catalyst fouling expressed as η/η_0 is insensitive to variations in the activation energy of the main reaction. This is consistent with previous conclusions that under these conditions the fouling is uniform and no significant intraparticle concentration or temperature gradients develop. For $\phi = 5$ there is some effect of

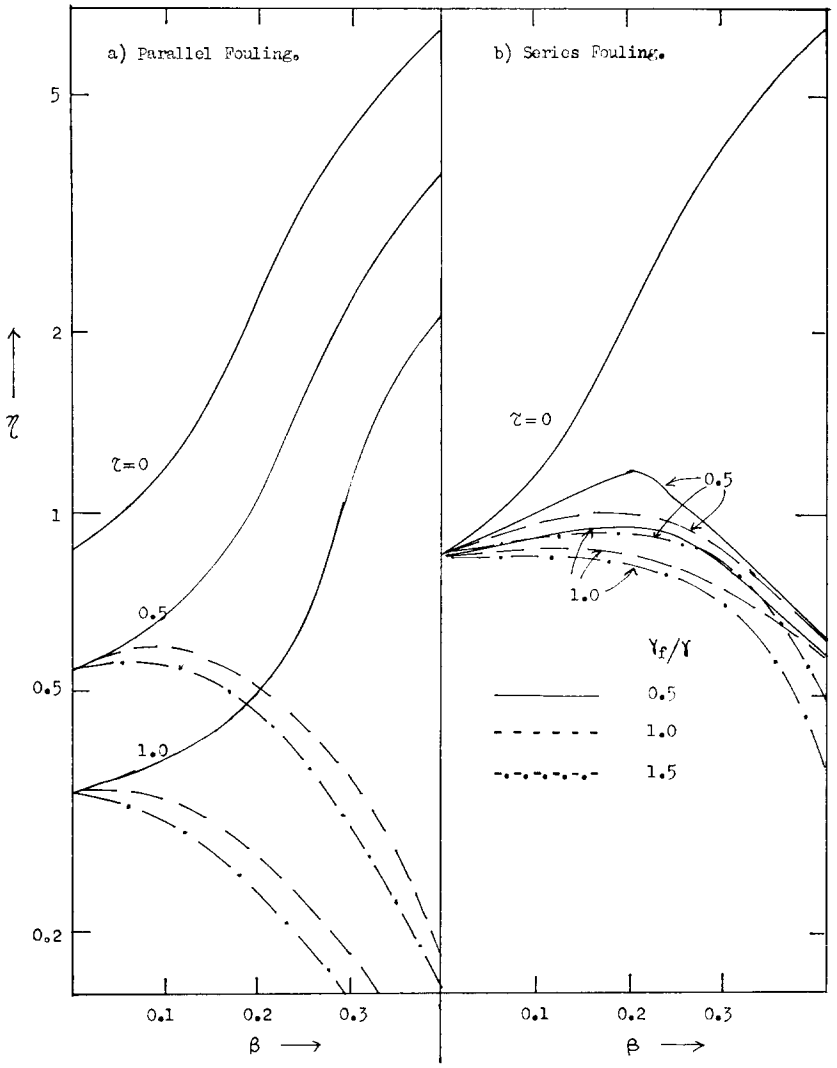

FIG. 8. Effect of thermicity factor β and activation energy ratio γ_f/γ on effectiveness factors. Data: $\gamma = 20$, $K_A^* = K_B^* = 10$, $h_{K_A} = h_{K_B} = 5$, $b_0 = 0$, and $\phi = 10$.

γ on fouling by a parallel mechanism but only at values of γ equal to 10 does this effect become really pronounced. For series fouling the parameter γ has virtually no effect at $\phi = 5$, while for $\phi = 10$, the effect is substantial for $\gamma = 30$ and only of marginal importance for $\gamma = 20$.

Adsorption Constants and Heats of Adsorption

The effect of the adsorption constant for reactant A and product B on the relative effectiveness of a fouled catalyst is shown in Fig. 10 for both parallel and series fouling for fouling times up to $\tau = 1.0$. In these computations equal activation energies were taken for the main and fouling reactions and equal heats of adsorption for reactant and product were also assumed. For parallel fouling the fouling increased with larger values of the dimensionless adsorption constants with the effect of an increase in K_A^* being of more importance than an increase in the adsorp-

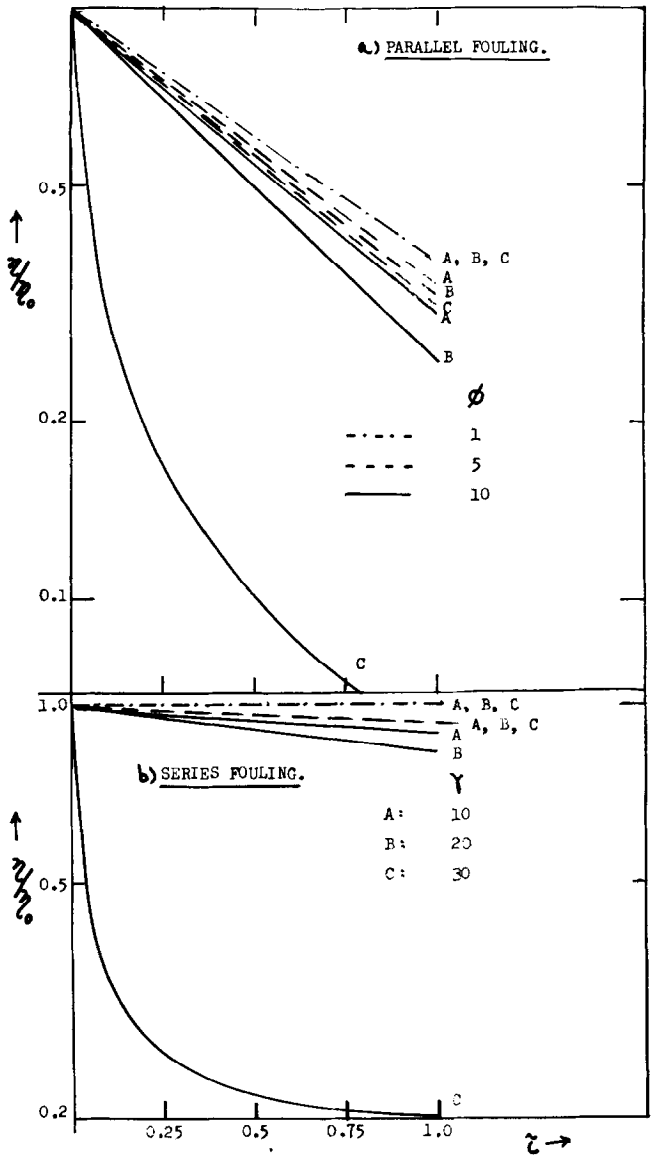

FIG. 9. Effect of γ. Effect of activation energy on effectiveness factor ratio. Data: $\gamma_f = 20$, $\beta = 0.2$, $K_A^* = 10$, $K_C^* = 10$, $b_0 = 0$, $h_{K_A} = 5$ and $h_{K_C} = 5$.

tion constant of product K_B^* (compare the different degree of deactivation between A — B and C — D). This is to be expected in view of the parallel reaction scheme assumed, whereby the fouling deposit is formed directly from reactant A and hence adsorption of A should facilitate fouling to the same extent as for the main reaction. For series fouling, Fig. 10 shows that adsorption appears to act in the opposite manner, increased values of the adsorption constants leading to more active catalysts, whereas values of K_A^* and K_B^* equal to zero give the greatest degree of fouling. This behavior arises from the use of Langmuir–Hinshelwood kinetics for cases

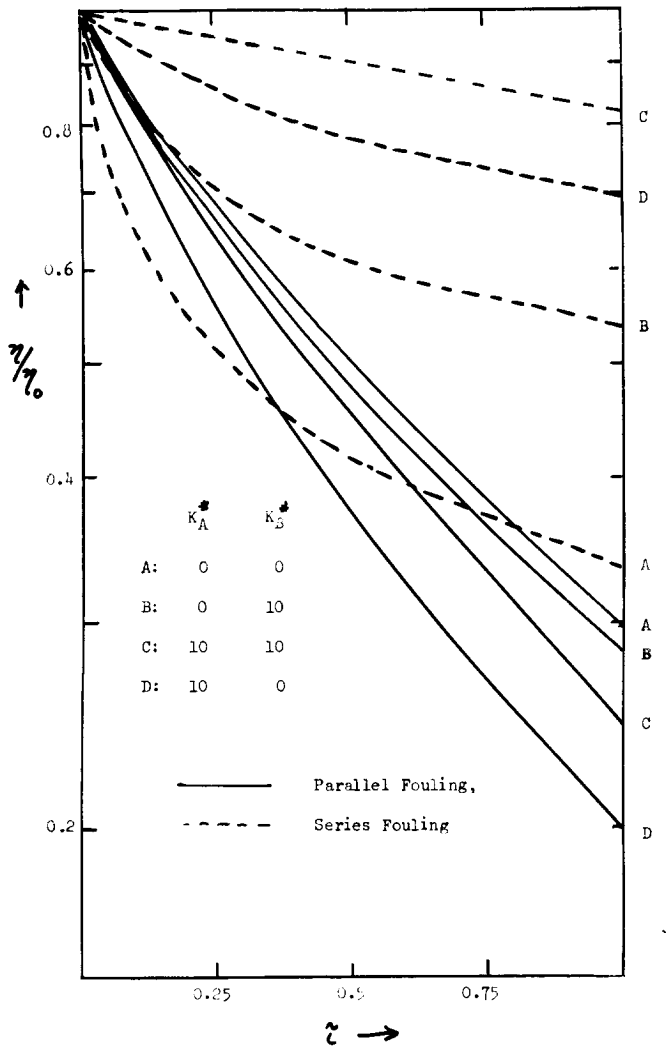

FIG. 10. Effect of K_A^* and K_B^*. Effect of adsorption equilibrium constants on effectiveness factor ratio. Data: $\gamma = \gamma_f = 20$, $\beta = 0.2$, $b_0 = 0$, $h_{K_A} = h_{K_B} = 5$, $\phi = 10$.

of fouling by a series mechanism where the precursor of the fouling deposit is the product of the reaction. For this type of fouling, simple first order kinetics ($K_A^* = K_B^* = 0$) would give the greatest decrease in reactant concentration on entering the pellet and therefore a larger increase in product concentration. This would give rise to increased fouling. Langmuir–Hinshelwood kinetics, being of an empirical order less than unity, would give decreased product concentration inside the catalyst pellet and would lead therefore to decreased fouling compared to first order kinetics.

The influence of the heats of adsorption for reactant and product, h_{K_A} and h_{K_B}, are shown in Fig. 11 for $\phi = 10$. It is seen that the relative extent of fouling, η/η_0, is affected to only a minor extent by changes in this parameter over the range investigated (0–10) although the value of η_0 is itself affected by changes in h_{K_A} and h_{K_B}.

Multiple Steady States in the Catalyst Pellets

It is well known that under certain conditions multiple steady states may occur within a single catalyst pellet [see

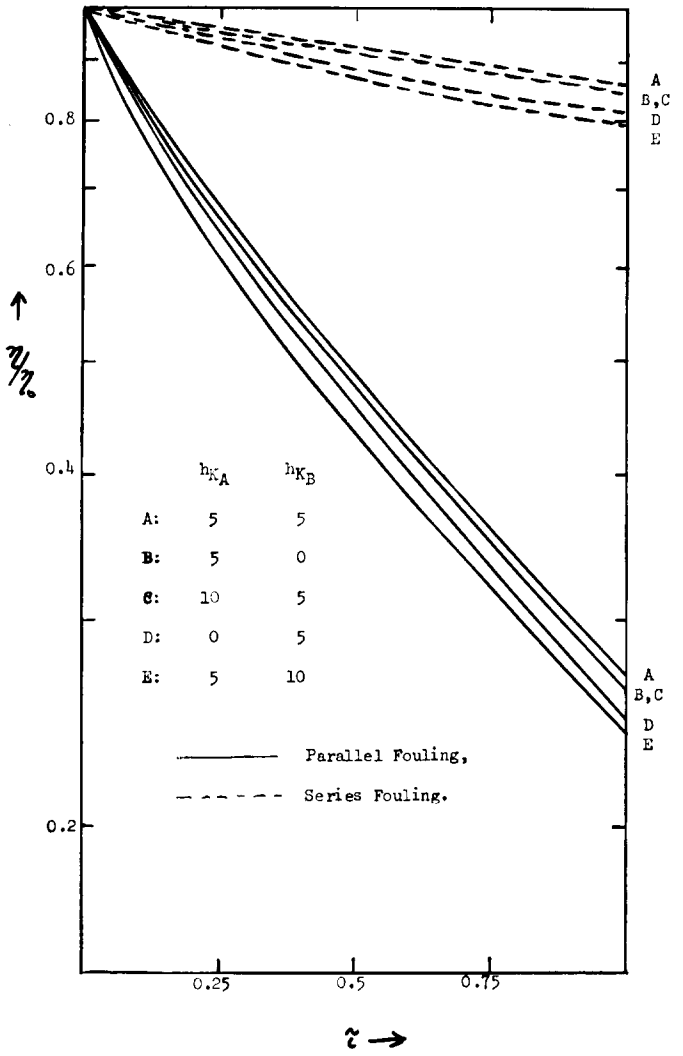

FIG. 11. Effect of h_{K_A} and h_{K_B}. Effect of heats of adsorption on effectiveness factor ratio. Data: $\gamma = \gamma_f = 20$, $\beta = 0.2$, $K_A^* = K_B^* = 10$, $b_0 = 0$, $\phi = 10$.

for example (*19*)] and the effect of fouling in this region has been investigated in this work. Multiple steady states occur for parallel fouling with the set of parameters $\beta = 0.3$, $\gamma = 30$, $K_A^* = K_B^* = 10$, $h_{K_A} = h_{K_B} = 5$ at a Thiele modulus to 2.2. The effect of fouling when the catalyst is operated in this multiple steady state region is illustrated in Fig. 12 where the effectiveness factor is plotted as a function of the fouling time. Three values of the particle effectiveness factor are shown corresponding to the upper and lower stable states (curves C and A, respectively) and an intermediate unstable steady state (curve B). The effectiveness factor at the lower steady state decreases slowly with increasing reaction time throughout the whole period considered. The upper steady state effectiveness also decreases monotonically with time initially (but at a faster rate than the lower steady state) but at a value of τ equal to 0.09, the effectiveness drops abruptly to a level below that

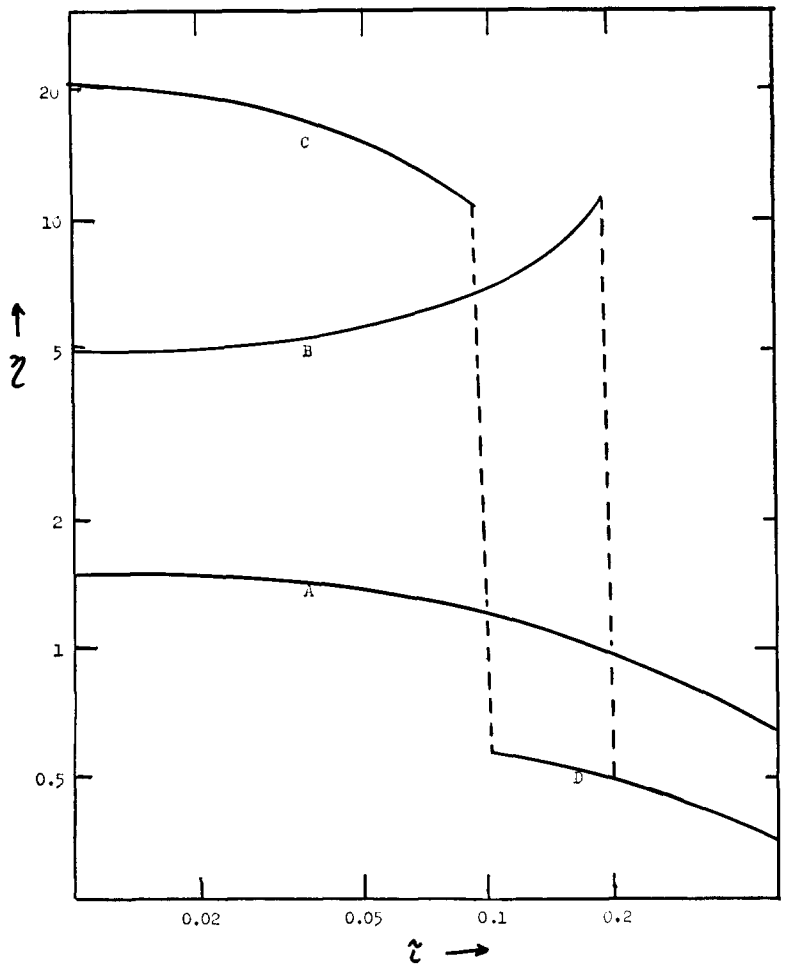

FIG. 12. η vs τ plots, multiple steady states. Effectiveness factors vs time for multiple steady state region. Data: $\gamma = 30$, $\gamma_f = 20$, $\beta = 0.3$, $K_A^* = K_B^* = 10$, $b_0 = 0$, $h_{K_A} = h_{K_B} = 5$, $\phi = 2.2$.

of the lower steady state. This behavior is explicable in terms of the variation with time of the mean dimensionless particle temperatures as shown in Fig. 13. The dimensionless temperatures at the lower stable steady state (curve A) are only slightly higher than the surface value and as fouling proceeds the particle temperature decreases slowly with time. At the upper stable steady state (curve C) the maximum value of the mean temperature is 1.2 at zero time and this decreases fairly rapidly with increasing reaction time up to $\tau = 0.09$. At this point a sudden steep drop in temperature occurs to curve D. The behavior of the intermediate steady state is interesting. The effectiveness factor and the mean pellet temperature (curve B) increase with fouling time despite the fact the fouling is taking place. Ultimately, both the effectiveness factor and the mean pellet temperature drop very suddenly at $\tau = 0.19$ to values below those for the lower steady state. From these results it would appear that continuous operation at the upper steady state may be difficult. If it is required to operate in this region of high conversion the optimal strategy would probably involve intermittent operation with frequent catalyst regeneration,

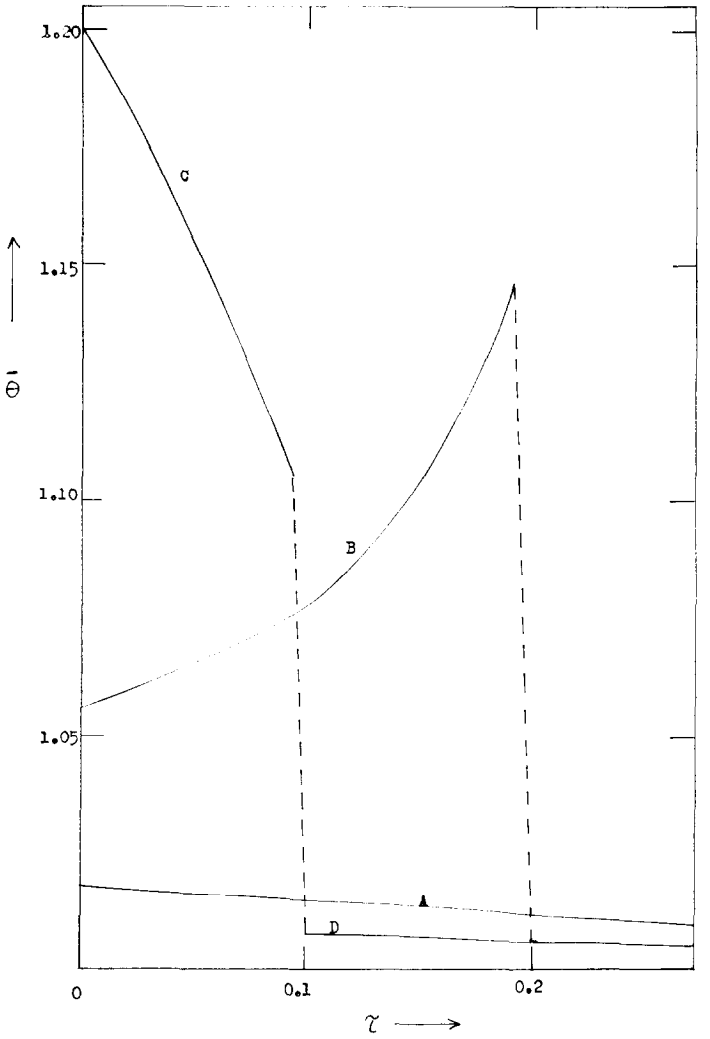

FIG. 13. Variation with time of the mean dimensionless temperature for the three steady states. Data: $\gamma = 30$, $\gamma_f = 20$, $\beta = 0.3$, $K_A^* = K_B^* = 10$, $h_{K_A} = h_{K_B} = 5$, $b_0 = 0$, $\phi = 2.2$.

the time between catalyst regenerations being determined from the appropriate effectiveness factor plots.

ACKNOWLEDGMENT

We are grateful to the Science Research Council for financial assistance which enabled this work to be carried out.

REFERENCES

1. Rudershausan, C. G., and Watson, C. C., *Chem. Eng. Sci.* **3**, 110 (1955).
2. Voorhies, A., *Ind. Eng. Chem.* **37**, 318 (1945).
3. Eberley, P. E., and Kimberlin, C. N., *Advan. Chem. Ser.* **109**, 506 (1972).
4. Hogan, J. P., Banks, R. L., and Lanning, W. C., *Ind. Eng. Chem.* **47**, 752 (1955).
5. Balder, J. R., and Petersen, E. E., *Chem. Eng. Sci.* **23**, 1287 (1968).
6. Greco, G., Jr., Alfani, F., and Gioia, F., *J. Catal.* **30**, 155 (1973).
7. Ogunye, A. F., Ray, W. H., *Advan. Chem. Ser.* **109**, 500 (1972).
8. Lin, S. H., *Biotech. Bioeng.* **17**, 1237 (1975).
9. Butt, J. B., *Advan. Chem. Ser.* **109**, 259 (1972).
10. Wheeler, A., *in* "Catalysis" (P. H. Emmett, Ed.), Vol. 2, Reinhold, New York, 1955.

11. Masamune, S., and Smith, J. M., *AIChE J.* **12,** 384 (1966).

12. Murakami, Y., Kobayashi, T., Hattori, T., and Masuda, M., *Ind. Eng. Chem. Fundam.* **7,** 599 (1968).

13. Chu, C., *Ind. Eng. Chem. Fundam.* **7,** 509 (1968).

14. Kam, E. K. T., Ramachandran, P. A., and Hughes, R., *J. Catal.* **38,** 283 (1975).

15. Khang, S. J., and Levenspiel, O., *Ind. Eng. Chem. Fundam.* **12,** 185 (1973).

16. Sagara, M., Masamune, S., and Smith, J. M., *AIChE J.* **13,** 1226 (1967).

17. Prater, C. D., *Chem. Eng. Sci.* **8,** 284 (1958).

18. Villadsen, J. V., and Stewart, W., *Chem. Eng. Sci.* **22,** 1483 (1967).

19. Weisz, P. B., and Hicks, J. S., *Chem. Eng. Sci.* **17,** 265 (1962).